POLYPUBLIE
Polytechnique Montréal

POLYTECHNIQUE MONTRÉAL
LE GÉNIE EN PREMIÈRE CLASSE

Document en libre accès dans PolyPublie
Open Access document in PolyPublie

Document publié chez l'éditeur officiel
Document issued by the official publisher

Full length article

Effects of porosity on seismic velocities, elastic moduli and Poisson's ratios of solid materials and rocks

Chengbo Yu [a], Shaocheng Ji [a,*], Qi Li [b]

[a] Département des Génies Civil, Géologique et des Mines, École Polytechnique de Montréal, Montréal, Québec, H3C 3A7, Canada
[b] State Key Laboratory of Geomechanics and Geotechnical Engineering, Institute of Rock and Soil Mechanics, Chinese Academy of Sciences, Wuhan, 430071, China

ARTICLE INFO

ABSTRACT

The generalized mixture rule (GMR) is used to provide a unified framework for describing Young's (E), shear (G) and bulk (K) moduli, Lame parameter (λ), and P- and S-wave velocities (V_p and V_s) as a function of porosity in various isotropic materials such as metals, ceramics and rocks. The characteristic J values of the GMR for E, G, K and λ of each material are systematically different and display consistent correlations with the Poisson's ratio of the nonporous material (ν_0). For the materials dominated by corner-shaped pores, the fixed point at which the effective Poisson's ratio (ν) remains constant is at $\nu_0 = 0.2$, and $J(G) > J(E) > J(K) > J(\lambda)$ and $J(G) < J(E) < J(K) < J(\lambda)$ for materials with $\nu_0 > 0.2$ and $\nu_0 < 0.2$, respectively. $J(V_s) > J(V_p)$ and $J(V_s) < J(V_p)$ for the materials with $\nu_0 > 0.2$ and $\nu_0 < 0.2$, respectively. The effective ν increases, decreases and remains unchanged with increasing porosity for the materials with $\nu_0 < 0.2$, $\nu_0 > 0.2$ and $\nu_0 = 0.2$, respectively. For natural rocks containing thin-disk-shaped pores parallel to mineral cleavages, grain boundaries and foliation, however, the ν fixed point decreases nonlinearly with decreasing pore aspect ratio (α: width/length). With increasing depth or pressure, cracks with smaller α values are progressively closed, making the ν fixed point rise and finally reach to the point at $\nu_0 = 0.2$.

© 2016 Institute of Rock and Soil Mechanics, Chinese Academy of Sciences. Production and hosting by Elsevier B.V. All rights reserved.

1. Introduction

Porosity is a fundamental microstructural parameter for most natural and man-made materials and influences significantly physical properties of these materials such as diffusion coefficient, elastic wave velocities, elastic moduli, Poisson's ratio, yield, rupture or ductile strength, thermal conductivity, electrical conductivity, fluid permeability, dielectric constant, magnetic permeability. Sediments and rocks (e.g. soils, sands and sandstone) are typical examples of natural porous materials. The main goal of this study is to calibrate the porosity-dependence of seismic velocities (e.g. P- and S-wave velocities: V_p and V_s), V_p/V_s ratio or Poisson's ratio, and elastic moduli of isotropic solid rocks because such a calibration is required to interpret correctly the geophysical data of natural resources (e.g. petroleum and natural gases). Such a calibration is also helpful to the understanding of the mechanical properties of geotectonical engineering materials that are equally porous.

Furthermore, foamed metals, sintered ceramics, hollow concretes and cellular polymers are man-made porous materials that have been widely used for thermal and acoustic insulation, impact energy absorption, vibration suppression, air or water filtration, fluid flow control, self-lubricating bearing, floatation and lightweight components. Therefore, to model accurately the mechanical properties of candidate solid materials in terms of their component properties, porosity and microstructure have broad significance for a wide range of fields from materials engineering to Earth sciences.

In the present study, our particular attention is paid to the influence of porosity on the compressional (P) and shear (S) wave velocities (V_p and V_s) as well as the Poisson's ratio, which is a function only to the ratio of V_p/V_s, of isotropic solid materials and rocks. The reason for this purpose is simple and given below. Direct observations on the nature of the materials that constitute the Earth are limited to studies of surface outcrops and rocks that have been obtained from mining and drilling. Drilling for mining and scientific purposes has penetrated to generally a few kilometers and the maximum to 10–12 km (10 km for the KTB hole in Germany, and 12 km for the Kola hole in Russia) beneath the surface, leaving much of the Earth's interior inaccessible. Much of our knowledge of the chemical composition, physical state and structure of the Earth's interior mainly comes from seismic data. Interpretation of these seismic data, in turn, is largely constrained by the extrapolation of laboratory-measured seismic properties of

relevant rocks thought to exist in a given geological and physical (i.e. pressure and temperature) environment. Apart from chemical composition, phase transformation, metamorphic reaction, dehydration, partial melting, temperature and pressure (e.g. Ji et al., 2002), porosity is a critical factor to affect the elastic wave properties of dry and wet rocks. However, the studies of this kind are extremely difficult because the geometrical shape, size distribution and connectivity of pores in three-dimensional, opaque rocks are generally unknown. Thus, the results from laboratory studies on the dependence of the elastic and seismic properties of isotropic man-made materials (e.g. metals, ceramics, and oxides) with known porosities may help to better understand seismic data from the natural rocks.

The elastic properties of an isotropic material or rock can be described by any two of the four elastic moduli termed Young's modulus (E), shear modulus (G), bulk modulus (K) and Lame parameter (λ). The Young's modulus (E) is defined as the ratio of the stress along an axis over the strain along that axis in the range of uniaxial stress in which Hooke's law holds. The bulk modulus (K) measures a substance's resistance to uniform compression while the shear modulus (G) is defined as the resistance to a simple shear strain that produces a shape change without changing total volume. The Lame parameter (λ) is quite special because it relates stresses and strains in perpendicular directions (Jaeger, 1969). The physical meaning of λ can be clearly illustrated in a special case of uniaxial strain where $\varepsilon_1 \neq 0$, and $\varepsilon_2 = \varepsilon_3 = 0$ (i.e. no displacement occurs in the direction perpendicular to the x-axis): $\lambda = \sigma_2/\varepsilon_1 = \sigma_3/\varepsilon_1$ (Ji et al., 2010). Goodway (2001) believed that λ is closely related to material's incompressibility ($\lambda = K - 2G/3$) and contains a higher proportion of information about the resistance to a change in volume caused by a change in pressure. The above 4 parameters (i.e. E, G, K and λ) are the most intrinsic elastic coefficients to express stress in terms of strain.

The most common geophysical parameters measurable are compressional (P) and shear (S) wave velocities (V_p and V_s) and densities (ρ) of elastic media. E, G, K and λ for isotropic elasticity can be easily determined from the measured seismic data:

$$V_p = \sqrt{\frac{K + \frac{4}{3}G}{\rho}} \tag{1}$$

$$V_s = \sqrt{\frac{G}{\rho}} \tag{2}$$

$$\nu = \frac{E}{2G} - 1 \tag{3}$$

$$K = \frac{E}{3(1 - 2\nu)} \tag{4}$$

$$\lambda = K - \frac{2}{3}G \tag{5}$$

where ν is the Poisson's ratio. $\lambda \leq 0$ if $V_p/V_s \leq \sqrt{2}$. $\lambda/G \geq 1$ if $V_p/V_s \geq \sqrt{3}$ (e.g. almandine, antigorite, calcite, dolomite, fayalite, feldspar, hematite, hornblende, lizardite, sillimanite, spinel, spessartine, talc, rutile, and wustite), and $0 \leq \lambda/G < 1$ if $\sqrt{2} \leq V_p/V_s < \sqrt{3}$ (e.g. quartz, bronzite, diallage, enstatite, forsterite, sapphire, periclase, and staurolite). The information about G and λ can be extracted from the inversion of P- and S-wave reflectivities (Estabrook and Kind, 1996; Goodway et al., 1997; Gray and Andersen, 2000; Goodway, 2001; Dufour et al., 2002; Gray, 2003; Li et al., 2003). Obviously, any two of these four moduli (E, G, K and λ) offer the most fundamental

parameterization of elastic seismic waves to extract information about the composition and structure of rocks in the Earth's interior. In the literature, however, only E, K, G and ν are usually reported although λ is also an intrinsic and invariant property of elastic media under given conditions. So far, little systematic research work has been carried out on the characterization of λ values for crystalline rocks and materials (Ji et al., 2010). Here we also calibrate the porosity-dependence of λ values for the solid materials of interest.

Poisson's ratio (ν) is the negative of the ratio of transverse strain to the axial strain when an isotropic material is subjected to uniaxial stress. For an isotropic material at a given temperature and a given pressure, ν is a constant which lies between -1 and 0.5. Materials with $\nu < 0$ are called auxetic materials because there is an increase in volume when compressed (Lakes, 1987). Here only the Poisson's ratios of isotropic materials are considered, which can be calculated from P- and S-wave velocities (V_p and V_s) in the isotropic material:

$$\nu = 0.5 - \frac{0.5}{(V_p/V_s)^2 - 1} \tag{6}$$

Among the elastic properties, Poisson's ratio is the least studied, but at the same time the most interesting only (Christensen, 1996; Gercek, 2007; Ji et al., 2009; Wang and Ji, 2009). For example, Poisson's ratio is a helpful hint to overcome the non-uniqueness of the interpretation of either V_p or V_s alone in terms of petrological composition (e.g. Ji et al., 2013a,b; Shao et al., 2014). The crustal Poisson's ratio information can be obtained from the analysis of teleseismic receiver functions using single station techniques (Clarke and Silver, 1993; Zandt and Ammon, 1995; Ji et al., 2009). The interpretation of such crustal Poisson's ratio results (e.g. Owens and Zandt, 1997; Chevrot and van der Hilst, 2000; Nair et al., 2006) has been largely based on an assumption that Poisson's ratio depends primarily on SiO_2 content (with more mafic rocks corresponding to higher ν values) and fluid content (Tarkov and Vavakin, 1982; Christensen, 1996; Owens and Zandt, 1997). As shown in Fig. 1a, the common silicate rocks form an arc-shaped trend line indicating that the Poisson's ratio increases with density as the lithology changes from granite, schist, felsic gneiss, through diorite-syenite, intermediate gneiss and metasediment, to gabbro-diabase, amphibolite, and mafic gneiss, and then decreases as the rocks become ultramafic in composition (i.e. pyroxenite and peridotite). However, the monomineralic rocks such as quartzite, serpentinite, anorthosite, limestone and marble are significantly deviated from the trend line (Ji et al., 2009). Sandstone has a chemical composition similar to quartzite but significantly a higher ν value than quartzite, indicating that ν increases with increasing porosity since $\nu = 0.08$ for quartz (Fig. 1b). The effects of porosity on the Poisson's ratio for the other types of natural rocks have not been studied in detail due to the lacking of experimental data over a wide range of porosities and pore geometry. Thus, one of the main goals of this investigation is to constrain the effects of porosity on the V_p/V_s ratio or the Poisson's ratio of porous materials and rocks.

2. Generalized mixture rule (GMR)

In the present study, we use the generalized mixture rule (GMR) (Ji, 2004; Ji et al., 2004) to model the variations of seismic velocities and elastic moduli as a function of porosity. The GMR is expressed as

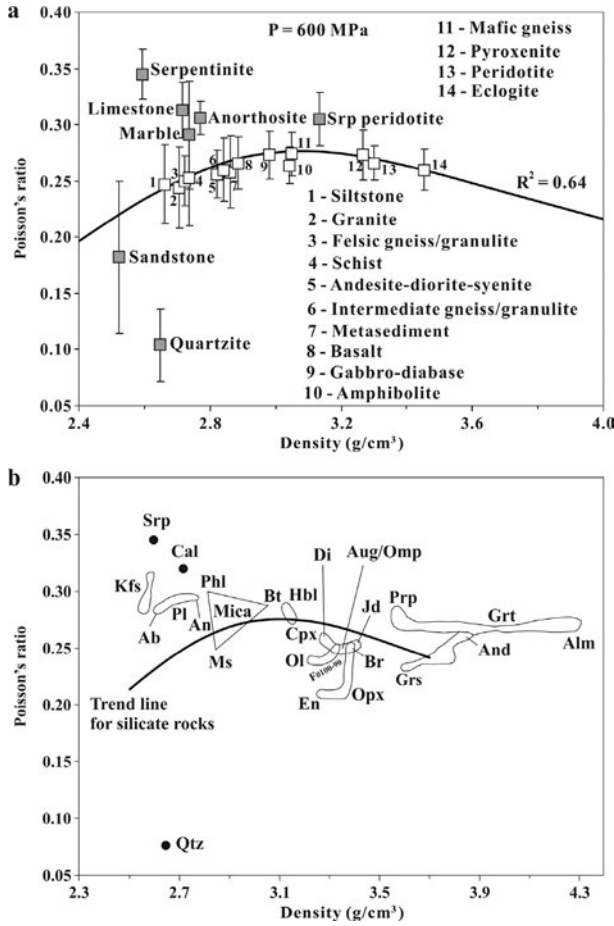$$M_c^J = \sum_{i=1}^{N} \left(V_i M_i^J \right) \tag{7}$$

Fig. 1. (a) Poisson's ratio-density plots for main categories of rocks. This figure was constructed based on the data from 620 samples, compiled in Handbook of Seismic Properties of Minerals, Rocks and Ores (Ji et al., 2002). The trend line was calculated from the correlations between the elastic moduli and density for 14 common lithologies (open squares) excluding the monomineralic rocks of serpentine, calcite and quartz (filled squares). (b) Poisson's ratio-density plots for main rock-forming minerals. Ab: albite; Alm: almandine; And: andradite; Aug: augite; Br: bronzite; Bt: biotite; Cal: calcite; Cpx: clinopyroxene; Di: diopside; En: enstatite; Grs: grossular; Grt: garnet; Hbl: hornblende; Jd: jadeite; Kfs: K-feldspar; Ms: muscovite; Ol: olivine; Omp: omphacite; Opx: orthopyroxene; Phl: phlogopite; Pl: plagioclase; Prp: pyrope; Qtz: quartz; Srp: serpentinite. The trend line is the same as that shown in (a).

where M is a measurable physical property (e.g. E, G, K, V_p and V_s); V is the volume fraction of component; the subscripts i and c represent, respectively, the ith phase and the composite consisting of N phases; and we have

$$\sum_{i=1}^{N} V_i = 1 \tag{8}$$

Effects of microstructures are expressed by a scaling, fractal parameter J, which is mainly controlled by the shape, size distribution, and distribution (continuity and connectivity) of the phases (Ji, 2004; Ji et al., 2004, 2006). Since then, the GMR has been widely used in the materials and Earth sciences (e.g. Pal, 2005; Takeda and Griera, 2006; Barzegari and Rodrigue, 2007; Yu and Wu, 2010; Culliton et al., 2013; DiRienzo et al., 2014).

According to Ji (2004) and Ji et al. (2006), $M_c(J)$ has the following characteristics:

(1) $M_c(J)$ is a continuous, strictly monotone function with respect to the volume fraction for all J values in the ranges $(-\infty, +\infty)$.

(2) For $J < 1$, $J = 1$ and $J > 1$, $M_c(J)$ as a function of the individual grades of membership M_i is strongly concave, linear, and strongly convex, respectively.

(3) For a binary system that consists of a strong phase (f) and a weak phase (m), $J < 0$ for the weak-phase supported structure while $J > 0$ for the strong-phase supported structure. The GMR fulfills the following boundary conditions: (i) For $V_f = 0$ (pure weak phase aggregate), the effective properties are equivalent to the properties of the weak phase for all values of J. (ii) For $V_f = 1$ (pure strong phase aggregate), the effective properties are equivalent to the properties of the strong phase for all values of J. (iii) For $V_f = V_m = 0.5$, we get the symmetric power means. (iv) In the circumstance that $M_f = M_m$ (two phases have an equivalent property), $M_c = M_f = M_m$ for all values of J and all values of V_f.

(4) The case $J = 1$ yields the arithmetic mean or Voigt average (which assumes constant strain). The case $J = -1$ yields the harmonic mean or Reuss average (which assumes constant stress). For isotropic composites, the Voigt and Reuss averages are generally regarded as the upper and lower bounds for effective elastic mechanical properties (e.g. E, G, K and λ) but not for effective seismic properties (e.g. V_p, V_s or Poisson's ratio). For the seismic properties (e.g. V_p, V_s or Poisson's ratio), the J values can be either higher than 1 or lower than -1. The GMR with $J \to 0$ yields the geometrical mean. However, the geometrical mean becomes physically meaningless when one of the constituent phases has a null property (e.g. in the case of porous materials). In this special case, the overall property of the composite acquired from the geometrical mean will always vanish regardless of the volume fraction of the constituent that has a null property (e.g. pores).

For a two-phase composite, Eq. (7) can be simplified:

$$M_c^J = (1 - V_m)M_f^J + V_m M_m^J \tag{9}$$

Porous materials are a special class of two-phase composites in which null strength pores are dispersed within a solid framework. Setting the mechanical property of the weak phase equal to zero (i.e. $M_m = 0$) and taking V_m as the volume fraction porosity (p) allow an estimation of the effect of porosity on the effective property (M_c). Eq. (9) can be written as

$$\frac{M_c}{M_s} = (1 - p)^{1/J} = V_s^{1/J} = \left(\frac{\rho_c}{\rho_s}\right)^{1/J} \tag{10}$$

where the subscript s represents the solid medium; and the parameter J depends on the geometrical shape, spatial arrangement, orientation and size distribution of pores, and in turn on the materials and the fabrication method (i.e. cold pressing, sintering, hot isostatic pressing, sedimentation and deformation); ρ_c and ρ_s are the densities of the porous and nonporous materials, respectively. ρ_c/ρ_s is the relative density that equals the volume fraction mass. The value of J lies in the range from 0 to 1 for any of the four elastic moduli (E, G, K, and λ). As mentioned before, the J value can be larger than 1 for seismic velocities (V_p and V_s) and Poisson's ratio. The variation of J with microstructure yields a large range of variations in elastic and seismic properties of porous solids. Clearly, the porosity has a greater effect on the properties at smaller values of J.

3. Experiments

In the literature of materials sciences, there is a significant amount of investigations on the effects of porosity on the seismic properties and the effective mechanical properties (e.g. elastic

moduli and strengths) of the materials. In the following, we will examine, using the GMR expressed in Eq. (10), the experimental results of the porous materials for which both P- and S-wave velocities and densities have been measured as a function of porosity so that the elastic moduli and Poisson's ratio can be calculated from the experimental results.

3.1. Silver compacts

Yeheskel et al. (2001) investigated experimentally the elastic wave velocities of silver compacts with porosities smaller than 0.33 using the pulse-echo method (Fig. 2). The pure silver without porosity has a density of 10.505 g/cm^3. Both P- and S-wave velocities can be well described by the GMR with $J(V_p) = 0.37$ ($R^2 = 0.96$) and $J(V_s) = 0.85$ ($R^2 = 0.952$), respectively, rather than the linear relations. $V_p/V_s = 2.477\exp(-1.782p)$ ($R^2 = 0.994$), corresponding to $\nu = 0.403\exp(-4.13p)$ ($R^2 = 0.893$). The GMR with $J(E) = 0.249$ ($R^2 = 0.992$), $J(G) = 0.298$ ($R^2 = 0.976$), $J(K) = 0.122$ ($R^2 = 0.963$), and $J(\lambda) = 0.104$ ($R^2 = 0.937$) provides excellent fitting for the dependences of the elastic moduli E, G, K and λ for the silver compacts (Fig. 2), which were calculated from the data of V_p, V_s and densities.

3.2. Iron compacts

Panakkal et al. (1990) measured the P- and S-wave velocities of iron compacts containing up to 22% porosities (Fig. 3). These compacts were prepared by hot isostatic pressing at 0.2−1.2 GPa and 1250 °C−1523 °C. The pore-free iron displays the following properties: $\rho = 7.86$ g/cm^3, $V_p = 6.089$ km/s and $V_s = 3.289$ km/s. The experimental data of V_p and V_s (Fig. 3) are in good agreement

with the values predicted by the GMR with $J(V_p) = 0.701$ ($R^2 = 0.945$) and $J(V_s) = 0.89$ ($R^2 = 0.967$). V_p/V_s decreases with increasing porosity: $V_p/V_s = 1.852\exp(-0.336p)$ ($R^2 = 0.997$), corresponding to $\nu = 0.294\exp(-0.82p)$ ($R^2 = 0.993$). The elastic moduli E, G, K and λ of the hot-pressed iron compacts can be well fitted by the GMR with $J(E) = 0.294$ ($R^2 = 0.979$), $J(G) = 0.308$ ($R^2 = 0.984$), $J(K) = 0.233$ ($R^2 = 0.949$), and $J(\lambda) = 0.205$ ($R^2 = 0.919$), respectively.

3.3. Porcelain

Boisson et al. (1976) reported ultrasonic velocities of sintered porcelain with porosities ranging from 0.09 to 0.37 (Fig. 4). The V_p and V_s values of the pore-free porcelain were estimated to be 7.811 km/s and 5.084 km/s, respectively. The best fitting of the experimental data using the GMR yields $J = 0.412$ ($R^2 = 0.969$) and 0.343 ($R^2 = 0.978$) for V_p and V_s, respectively (Fig. 4b). V_p/V_s increases with increasing porosity (Fig. 4b): $V_p/V_s = 1.536\exp(0.584p)$ ($R^2 = 0.991$). The elastic moduli E, G, K and λ of the porous porcelains can be well described by the GMR with $J(E) = 0.155$ ($R^2 = 0.981$), $J(G) = 0.146$ ($R^2 = 0.984$), $J(K) = 0.202$ ($R^2 = 0.957$) and $J(\lambda) = 0.325$ ($R^2 = 0.816$) (Fig. 4c), respectively. The Poisson's ratio increases with increasing porosity under the experimental conditions (Fig. 4d): $\nu = 0.132\exp(2.602p)$ ($R^2 = 0.995$).

3.4. Fused glass beads

Berge et al. (1995) measured P- and S-wave velocities in order to investigate the elastic properties of synthetic sandstone using sintered glass beads (71%−74% SiO_2, 12%−15% NaO_2, 8%−10% CaO, 1.5%−3.8% MgO, 0.2%−1.5% Al_2O_3, and 0%−0.2% K_2O, all in weight
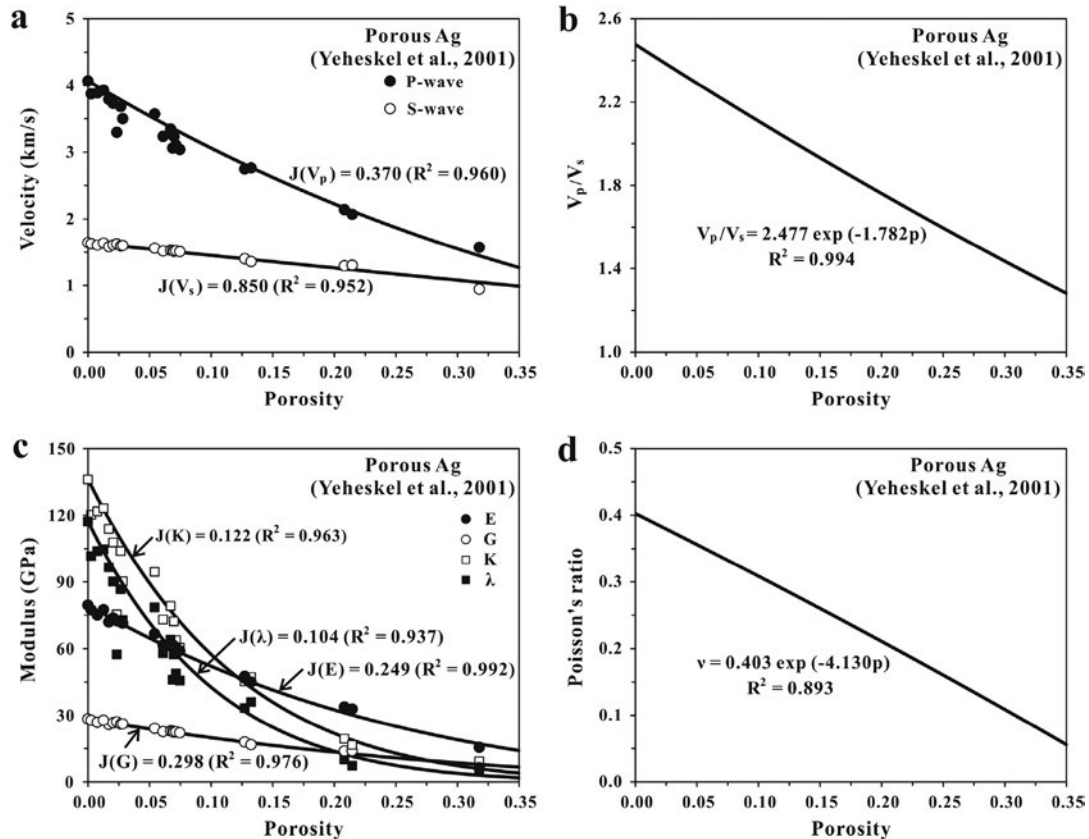

Fig. 2. Seismic wave velocities (a), V_p/V_s ratio (b), elastic moduli (c) and Poisson's ratio (d) of silver compacts as a function of porosity. GMR curves labeled according to J values.
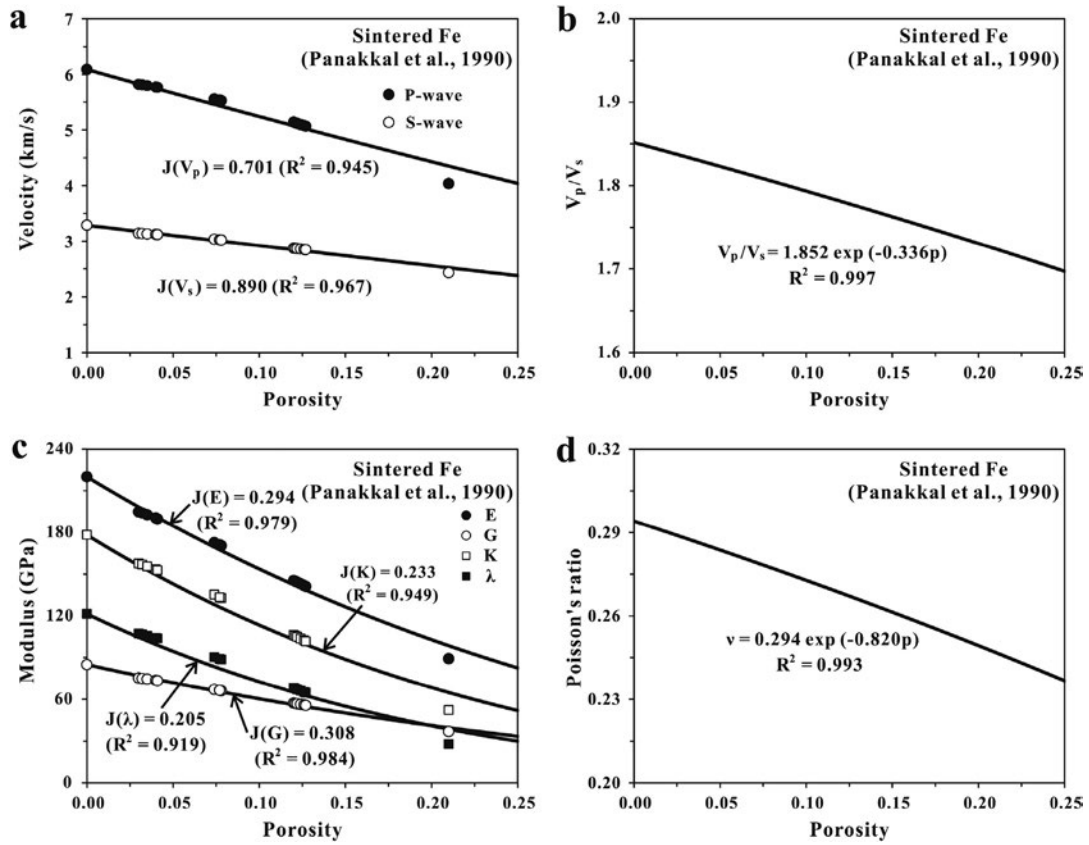
Fig. 3. Seismic wave velocities (a), V_p/V_s ratio (b), elastic moduli (c) and Poisson's ratio (d) of hot-pressed iron compacts as a function of porosity. GMR curves labeled according to J values.
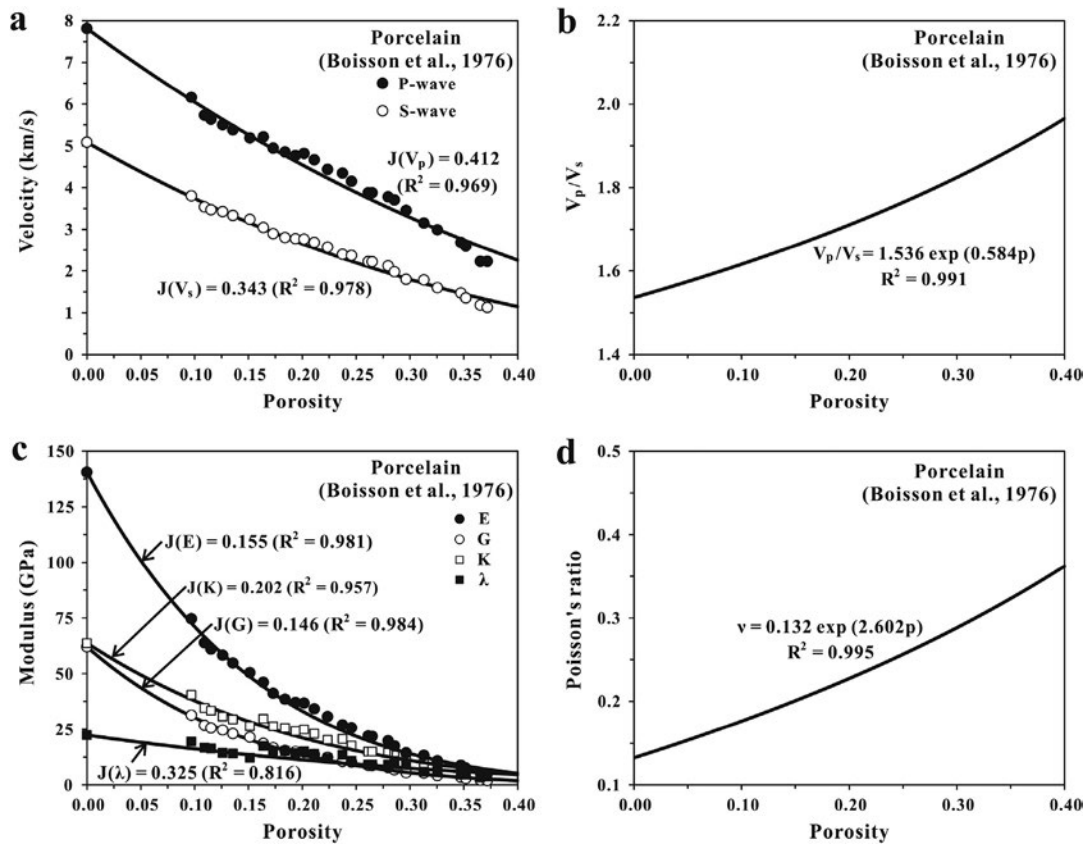

Fig. 4. Seismic wave velocities (a), V_p/V_s ratio (b), elastic moduli (c) and Poisson's ratio (d) of porcelain as a function of porosity. GMR curves labeled according to J values.

percent) with porosities ranging from 0.01 to 0.43. The fully dense glass shows: $\rho = 2.48$ g/cm^3, $V_p = 5.86$ km/s, $V_s = 3.43$ km/s, $V_p/V_s = 1.707$, $\nu = 0.239$, $E = 72.33$ GPa, $G = 29.2$ GPa, $K = 46.1$ GPa, and $\lambda = 26.63$ GPa. As shown in Fig. 5, clear drops of the seismic wave velocities and elastic moduli occur towards a critical porosity of ~ 0.3. For porosities below ~ 0.3, the samples are believed to have similar microstructures with isolated pores embedded in a continuous solid glass and the experimental data can be well described by the GMR (Eq. (10)) with $J(E) = 0.4$ ($R^2 = 0.993$), $J(G) = 0.403$ ($R^2 = 0.992$), $J(K) = 0.386$ ($R^2 = 0.957$) and $J(\lambda) = 0.37$ ($R^2 = 0.872$). The critical porosity presumably coincides with the minimum porosity for near-closely packed quasi-identical spheres. The J values for E and G decrease progressively from ~ 0.4 to ~ 0.25 with increasing porosity from 0.3 to 0.43, reflecting that the geometry of pores in the synthetic sandstone (fused glass beads) becomes complex due to the interaction between pores in this range of porosities.

3.5. SiO$_2$ glass

The sound velocities, densities and elastic moduli of porous SiO$_2$ glass samples with a wide range of porosities from 0 to 0.726 were reported in Adachi and Sakka (1990). The diameters of pores vary from 5 nm to 35 nm with an average value of about 16 nm. As shown in Fig. 6a, the GMR with $J(V_p) = 1.067$ ($R^2 = 0.984$) and $J(V_s) = 1.047$ ($R^2 = 0.985$) gives good predictions of the V_p and V_s variations over the wide range of porosity. The V_p/V_s ratio (Fig. 6b) increases slightly with increasing porosity: $V_p/V_s = 1.57\exp(0.029p)$ ($R^2 = 0.934$), corresponding to $\nu = 0.159\exp(0.186p)$ ($R^2 = 0.956$), indicating that ν increases with increasing porosity for this

material. Moreover, the linear expression used by previous authors (e.g. Panakkal et al., 1990; Panakkal, 1991) is disqualified for describing either the V_p/V_s or the Poisson's ratio data of the porous silica glasses. The experimental data of E, G, K and λ (Fig. 6c) essentially track the theoretical curves predicted by the GMR with $J(E) = 0.346$ ($R^2 = 0.993$), $J(G) = 0.344$ ($R^2 = 0.993$), $J(K) = 0.353$ ($R^2 = 0.992$) and $J(\lambda) = 0.366$ ($R^2 = 0.99$), respectively. It is important to note that there is no clear drop of the elastic moduli over the wide porosity range from 0 to 0.726, indicating that the samples have similar microstructures with isolated pores embedded in a continuous solid glass and the pores have not formed interconnected channels.

3.6. Alumina (Al$_2$O$_3$)

Asmani et al. (2001) investigated the influence of porosity on the compression and shear wave velocities in alumina ceramics containing porosities ranging from 0.02 to 0.25 (Fig. 7). In the pure alumina without porosity, $V_p = 10.904$ km/s and $V_s = 6.399$ km/s. The experimental data are consistent with the GMR with $J(V_p) = 0.882$ ($R^2 = 0.994$) and $J(V_s) = 1.046$ ($R^2 = 0.981$). $V_p/V_s = 1.704\exp(-0.202p)$ ($R^2 = 0.996$), corresponding to $\nu = 0.237\exp(-0.803p)$ ($R^2 = 0.989$). The Young's, shear and bulk moduli and the Lame parameter of the alumina ceramics, computed from ultrasonic velocities and densities, are plotted in Fig. 7c. The elastic properties can be well fitted by the GMR curves of $J(E) = 0.329$ ($R^2 = 0.994$), $J(G) = 0.343$ ($R^2 = 0.991$), $J(K) = 0.278$ ($R^2 = 0.998$) and $J(\lambda) = 0.241$ ($R^2 = 0.994$). The GMR is much better than the linear relation used by Asmani et al. (2001) for describing the dependence of the elastic moduli on the porosity.
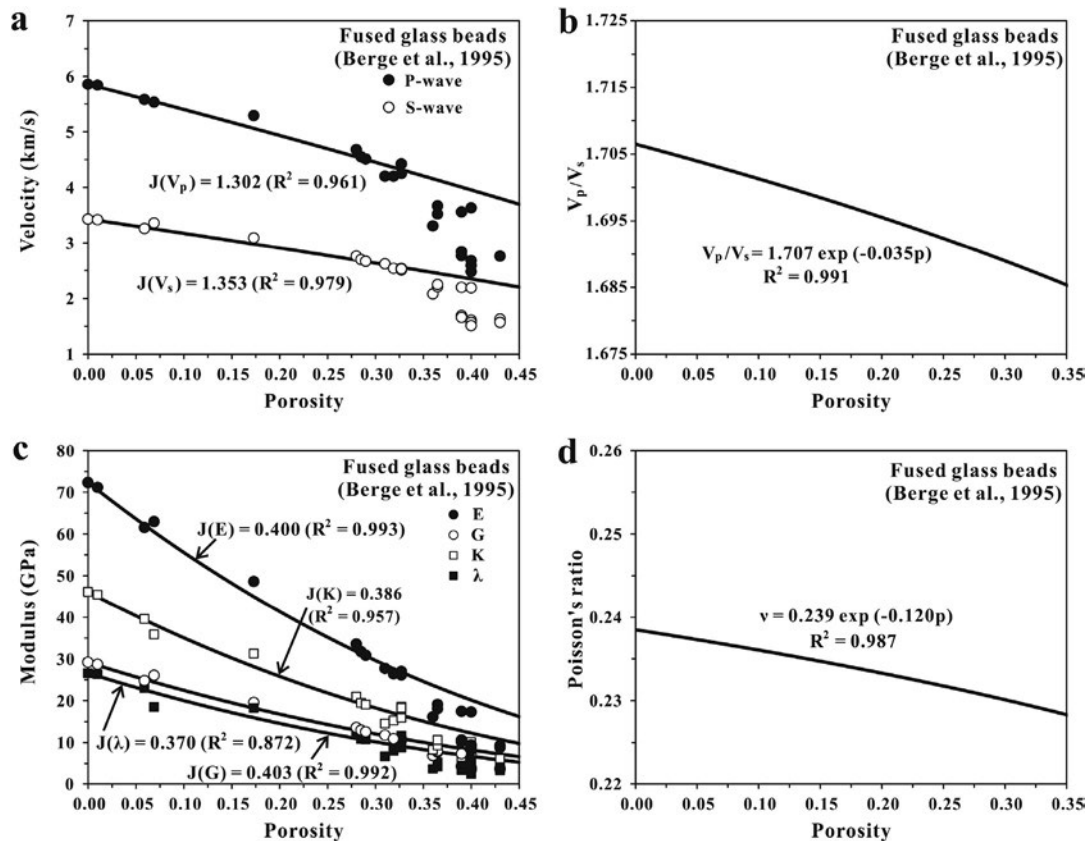

Fig. 5. Seismic wave velocities (a), V_p/V_s ratio (b), elastic moduli (c) and Poisson's ratio (d) of fused glass beads as a function of porosity. GMR curves labeled according to J values.
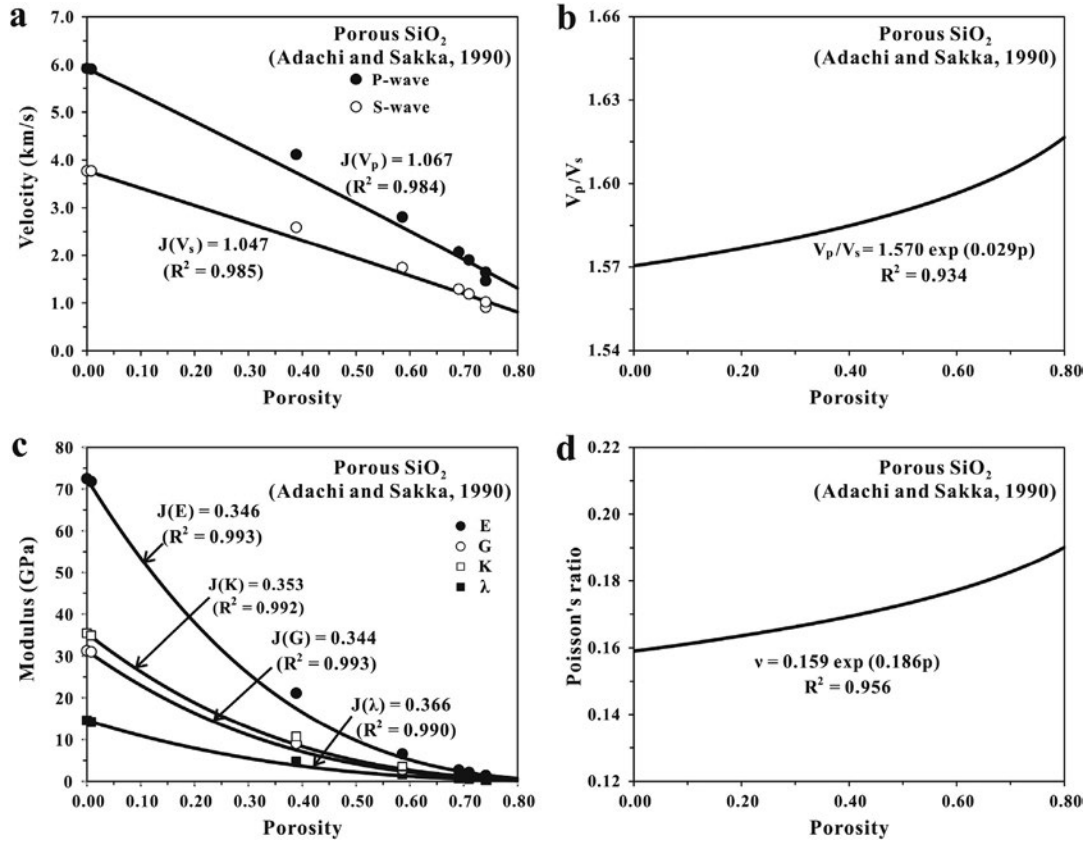
Fig. 6. Seismic wave velocities (a), V_p/V_s ratio (b), elastic moduli (c) and Poisson's ratio (d) of porous SiO$_2$ glasses as a function of porosity. GMR curves labeled according to J values.
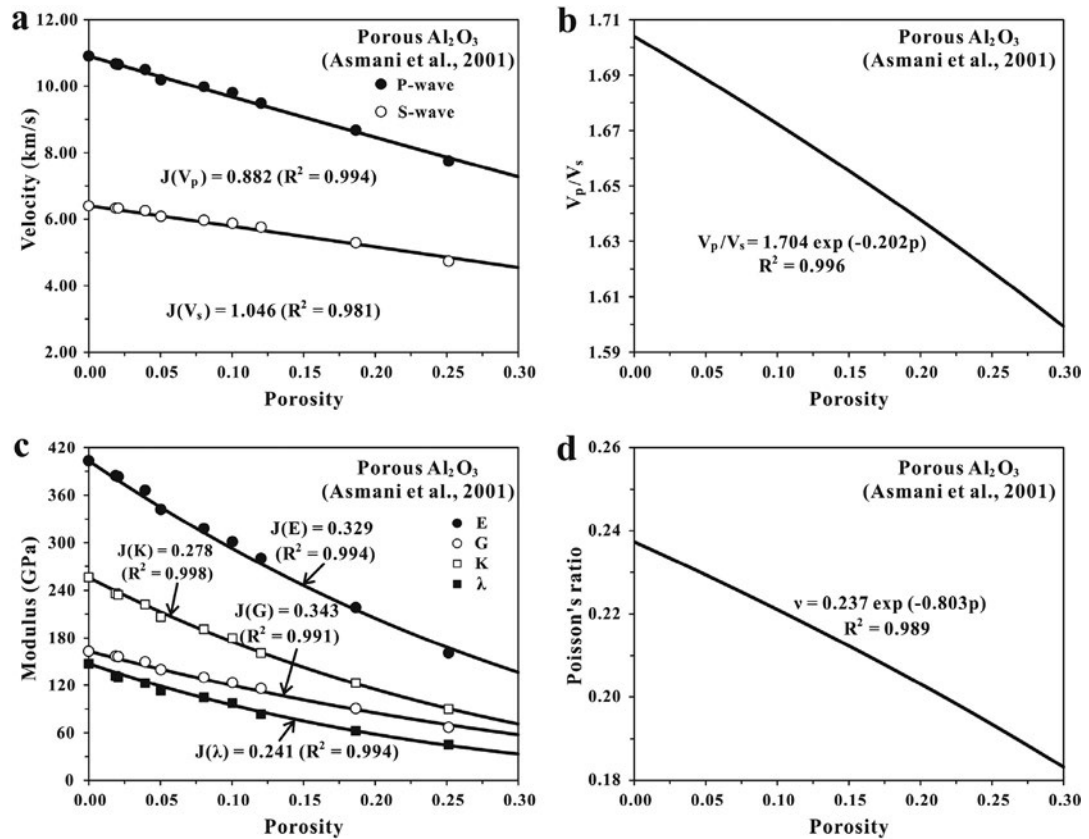

Fig. 7. Seismic wave velocities (a), V_p/V_s ratio (b), elastic moduli (c) and Poisson's ratio (d) of Al$_2$O$_3$ aggregates as a function of porosity. GMR curves labeled according to J values.

3.7. Periclase (MgO)

Fig. 8 demonstrates the sound velocity and Poisson's ratio data of polycrystalline MgO aggregates with porosities up to 5% (Soga and Schreiber, 1968). The least-squares fit using the GMR for the experimental data of MgO yields that $J(V_p) = 1.163$ ($R^2 = 0.973$) and $J(V_s) = 0.966$ ($R^2 = 0.991$). The V_p/V_s ratio increases with increasing porosity: $V_p/V_s = 1.6\exp(0.178p)$ ($R^2 = 1$), corresponding to $\nu = 0.18\exp(1.003p)$ ($R^2 = 1$). The elastic moduli E, G, K and λ can be well described by the GMR with $J(E) = 0.343$ ($R^2 = 0.994$), $J(G) = 0.326$ ($R^2 = 0.996$), $J(K) = 0.426$ ($R^2 = 0.964$), $J(\lambda) = 0.665$ ($R^2 = 0.746$) over the range of porosity from 0 to 0.05 (Fig. 8). There is a tendency that $J(\lambda) > J(K) > J(E) > J(G)$.

3.8. Spinel (MgAl₂O₄)

Fig. 9 illustrates the variation in the P- and S-wave velocities in hot-pressed spinel (MgAl₂O₄) aggregates (Porter et al., 1977). The GMR with $J(V_p) = 0.726$ ($R^2 = 0.959$), $J(V_s) = 0.828$ ($R^2 = 0.978$), $J(E) = 0.284$ ($R^2 = 0.991$), $J(G) = 0.293$ ($R^2 = 0.989$), $J(K) = 0.247$ ($R^2 = 0.947$) and $J(\lambda) = 0.221$ ($R^2 = 0.889$) provides statistically meaningful descriptions for the wave velocities and elastic moduli. Scatter in the velocity or modulus data shown in the plots (Fig. 9) can be attributed to variations in shape, size, and spatial distributions and orientations of micropores within the samples. For the spinel aggregates, $V_p/V_s = 1.76\exp(-0.199p)$ ($R^2 = 0.994$), corresponding to $\nu = 0.262\exp(-0.653p)$ ($R^2 = 0.969$).

3.9. Clean sandstone

Han (1986) measured both P- and S-wave velocities of 10 natural, dry, clean sandstones which consist of nearly pure quartz grains without clay (Fig. 10). Their V_p and V_s data as a function of porosity can be described by the GMR with $J(V_p) = 0.714$ ($R^2 = 0.992$) and $J(V_s) = 0.59$ ($R^2 = 0.988$), respectively. The elastic moduli calculated from the measured velocity and density data ($\rho_0 = 2.65$ g/cm³) also follow the theoretical curves of the GMR with $J(E) = 0.246$ ($R^2 = 0.995$), $J(G) = 0.228$ ($R^2 = 0.993$), $J(K) = 0.328$ ($R^2 = 0.986$), and $J(\lambda) = 2.091$ ($R^2 = 0.288$). The quartz sandstones display a clear increase in either V_p/V_s or ν: $V_p/V_s = 1.494\exp(0.326p)$ ($R^2 = 0.997$) and $\nu = 0.094\exp(3.202p)$ ($R^2 = 0.994$). This observation is consistent with the comparison between the Poisson's ratios of pore-free quartzite and porous quartz sandstones (Ji et al., 2009). These authors investigated 7 quartzite and 9 sandstone samples and obtained $\nu = 0.104$ for quartzite ($V_p = 5.951$ km/s and $V_s = 3.991$ km/s) and $\nu = 0.182$ for sandstone ($V_p = 5.097$ km/s and $V_s = 3.243$ km/s).

4. Discussion

Fig. 11a plots $J(V_s)$ versus $J(V_p)$ data from the experiments described above together with the results of SiC (Jeong and Hsu, 1996), titanium aluminide (Matikas et al., 1997), ZnO (Martin et al., 1996), UO₂ (Panakkal, 1991), 3Y-TZP ceramics (Luo and Stevens, 1999), Gd₂O₃ (Haglund and Hunter, 1973), Sm₂O₃ (Hunter et al., 1974), HfO₂ (Dole et al., 1977), ZrO₂ (Smith and Crandall, 1964), Lu₂O₃ (Hunter and Graddy, 1976) and Si₃N₄
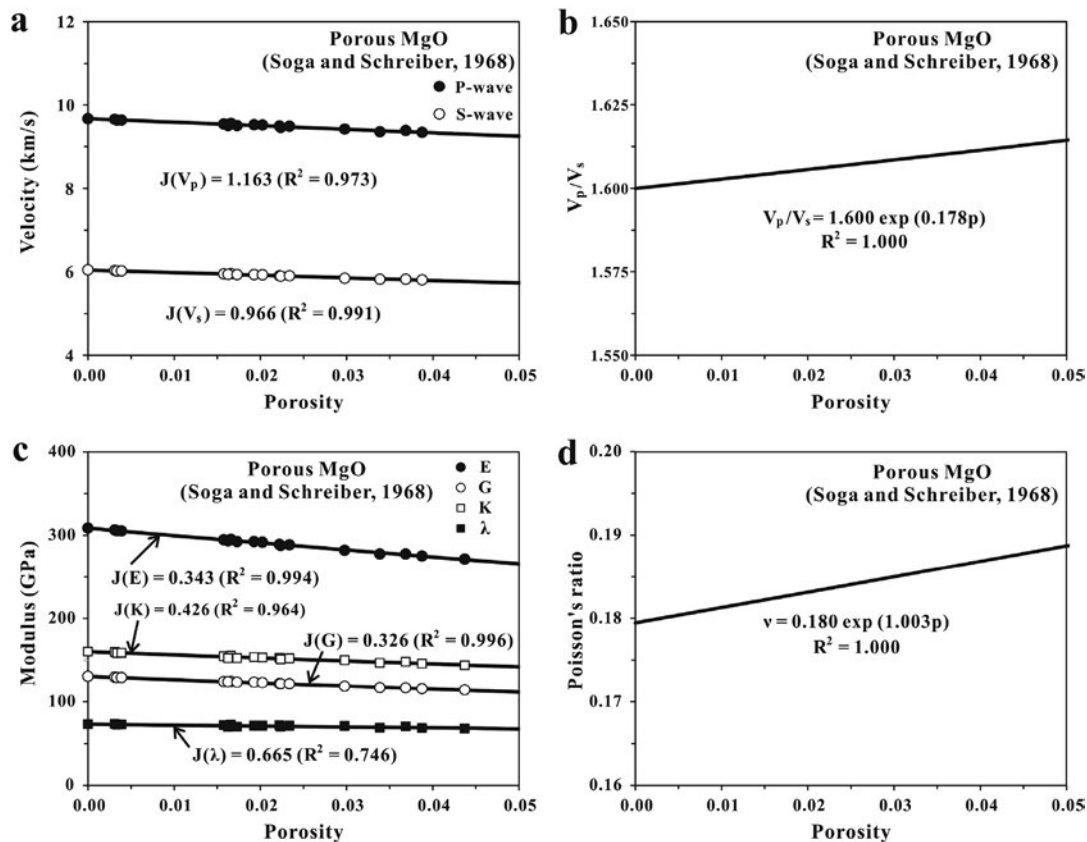
Fig. 8. Seismic wave velocities (a), V_p/V_s ratio (b), elastic moduli (c) and Poisson's ratio (d) of periclase (MgO) aggregates as a function of porosity. GMR curves labeled according to J values.
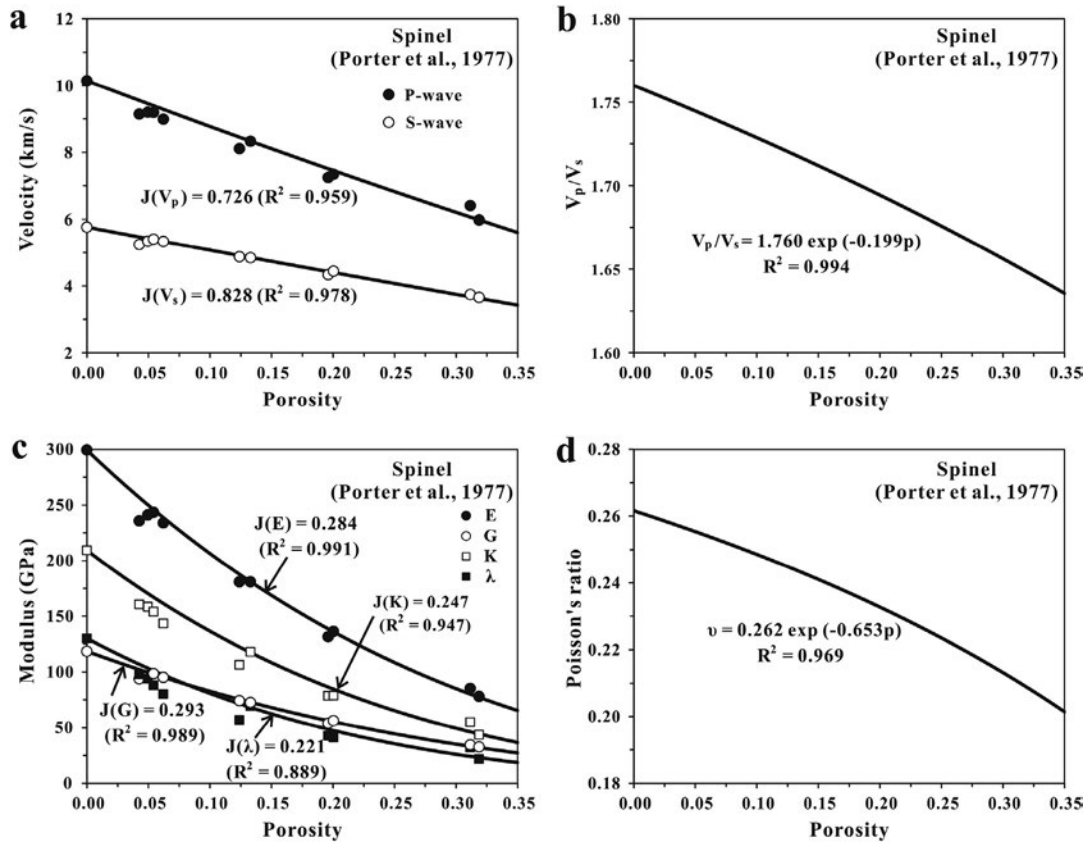
Fig. 9. Seismic wave velocities (a), V_p/V_s ratio (b), elastic moduli (c) and Poisson's ratio (d) of polycrystalline spinel aggregates as a function of porosity. GMR curves labeled according to J values.
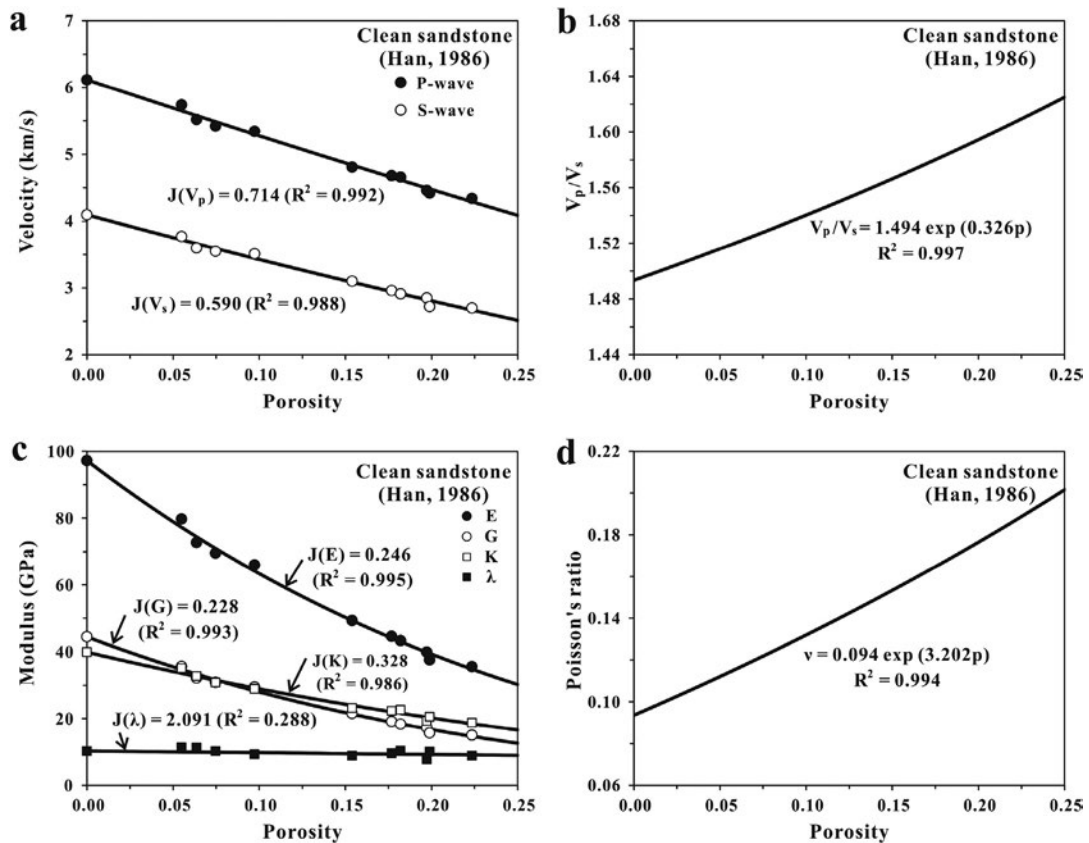

Fig. 10. Seismic wave velocities (a), V_p/V_s ratio (b), elastic moduli (c) and Poisson's ratio (d) of quartz sandstones as a function of porosity. GMR curves labeled according to J values.
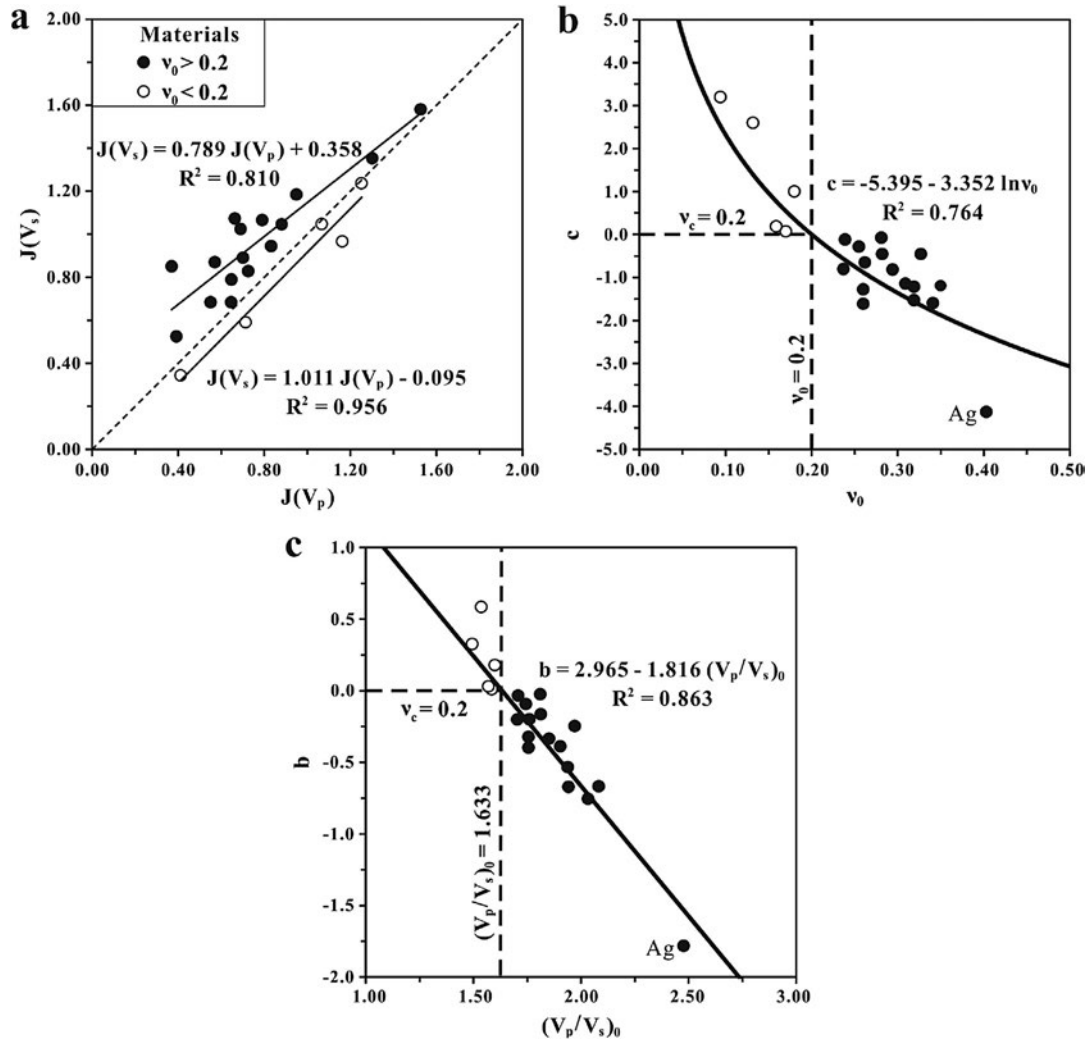
Fig. 11. Plots of $J(V_s)$ versus $J(V_p)$ (a), c value versus ν_0 (b), and b value versus $(V_p/V_s)_0$ (c). Solid dots: $\nu_0 > 0.2$; Open dots: $\nu_0 < 0.2$.

(McLean and Fisher, 1981). It is interesting to find that $J(V_s) > J(V_p)$ for the porous materials with $\nu_0 > 0.2$ (solid dots in Fig. 11) whereas $J(V_s) < J(V_p)$ for those porous materials with $\nu_0 < 0.2$ (open circles in Fig. 11). For those materials with $\nu_0 \approx 0.2$, $J(V_s) \approx J(V_p)$.

For the variation of effective Poisson's ratio (ν_c) as a function of porosity, described by $\nu_c = \nu_0 \exp(cp)$, we plotted c as function of ν_0 (Fig. 11b) and obtained the following correlation: $c = -5.395 - 3.352\ln\nu_0$ ($R^2 = 0.764$). When $\nu_0 = 0.2$, the effective Poisson's ratio becomes independent on the porosity. However, $c > 0$ (i.e. the effective Poisson's ratio increases with the porosity) and $c < 0$ (i.e. the effective Poisson's ratio decreases with the porosity) when $\nu_0 < 0.2$ and $\nu_0 > 0.2$, respectively. For the relation $(V_p/V_s)_c = (V_p/V_s)_0 \exp(bp)$, the b–$(V_p/V_s)_0$ plots (Fig. 11c) yield a linear relation: $b = 2.965 - 1.816(V_p/V_s)_0$ ($R^2 = 0.863$). When $(V_p/V_s)_0 = 1.633$, corresponding to $\nu_0 = 0.2$, the $(V_p/V_s)_c$ remains unchanged with the variation of the porosity. However, $b > 0$ (i.e. $(V_p/V_s)_c$ increases with the porosity) and $b < 0$ (i.e. $(V_p/V_s)_c$ decreases with the porosity) when $(V_p/V_s)_0 < 1.633$ and $(V_p/V_s)_0 > 1.633$, respectively.

Fig. 12 shows that the J values for the elastic moduli (E, G, K and λ) vary with the elastic wave velocities (V_p and V_s) in quite different manner. $J(K)$ displays an excellent correlation with $J(V_p)$ for the materials with $\nu_0 > 0.2$ (Fig. 12c) while such a linear correlation becomes deteriorated between $J(K)$ and $J(V_s)$ (Fig. 12g).

The dependences of $J(E)$ on $J(V_p)$ and $J(V_s)$ are nonlinear and linear, respectively. The correlations between $J(E)$ and $J(V_s)$ (Fig. 12e) and particularly those between $J(G)$ and $J(V_s)$ are nearly the same for the materials with any ν_0 values (>0.2 or <0.2, Fig. 12f). However, the correlations between $J(E)$ and $J(V_p)$ and those between $J(G)$ and $J(V_p)$ are remarkably different for the materials with $\nu_0 > 0.2$ and $\nu_0 < 0.2$ (Fig. 12a–b). The $J(\lambda)$ demonstrates nicely a linear relationship with $J(V_p)$ for the materials with $\nu_0 > 0.2$ (Fig. 12d). There are generally large scatters in the data of the materials with $\nu_0 < 0.2$.

It is important to note that $J(G) > J(E) > J(K) > J(\lambda)$ for all the materials with $\nu_0 > 0.2$ while $J(G) < J(E) < J(K) < J(\lambda)$ for all the materials with $\nu_0 < 0.2$ (Fig. 13). For the materials $\nu_0 = 0.2$, $J(G) = J(E) = J(K) = J(\lambda)$. As shown in Fig. 13a, the plots of $J(G)$ versus $J(E)$ all lie near the line $J(G) = J(E)$, but those for the porous solids with $\nu_0 > 0.2$ and $\nu_0 < 0.2$ occur above and below the line, respectively. $J(G) = 0.936J(E) + 0.035$ ($R^2 = 0.965$) and $J(G) = 1.029J(E) - 0.018$ ($R^2 = 0.994$) for the materials with $\nu_0 > 0.2$ and $\nu_0 < 0.2$, respectively. In other words, $J(E) > J(G)$ for all the materials with $\nu_0 > 0.2$ while $J(E) < J(G)$ for the materials $\nu_0 < 0.2$. As shown in Fig. 13b–f, $J(K) < J(E)$, $J(K) < J(G)$, $J(\lambda) < J(E)$, $J(\lambda) < J(G)$ and $J(\lambda) < J(K)$ for the solids with $\nu_0 > 0.2$. In contrast, $J(K) > J(E)$, $J(K) > J(G)$, $J(\lambda) > J(E)$, $J(\lambda) > J(G)$ and $J(\lambda) > J(K)$ for the solids with $\nu_0 < 0.2$.
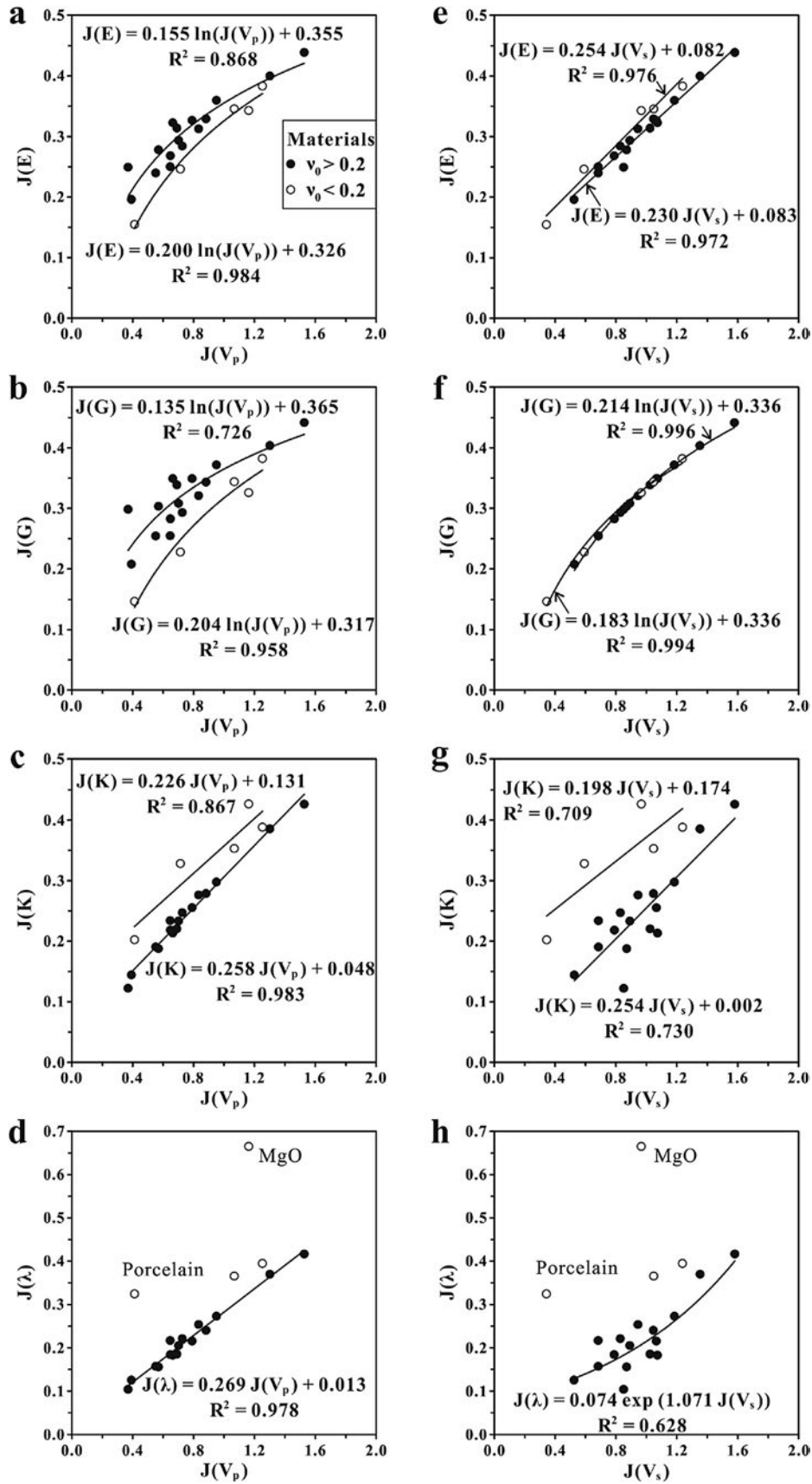
Fig. 12. Correlations of the $J(E)$, $J(G)$, $J(K)$ and $J(\lambda)$ with $J(V_p)$ and $J(V_s)$ for the porous materials studied. Solid dots: $v_0 > 0.2$; Open dots: $v_0 < 0.2$.

Substituting Eq. (10) into Eq. (3), we obtain:

$$\nu_c = (\nu_0 + 1)(1-p)^{1/J(E)-1/J(G)} - 1 \qquad (11)$$

where $1-p$ is always less than or equal to 1.

(1) If $J(G) > J(E)$ (the materials with $\nu_0 > 0.2$, Fig. 12a), $(1-p)^{1/J(E)-1/J(G)} < 1$, then $\nu < \nu_0$, that is, an increase in

porosity will always lead to a decrease in Poisson's ratio (Figs. 2, 3, 5, 7, 9). In the crust, an increase in hydrostatic pressure (or depth) will lead to a reduction in porosity, and thus an increase in the effective Poisson's ratios of the rocks with $\nu_0 > 0.2$ (e.g. amphibolite, gabbro, mafic granulite, peridotite, and serpentinite).

(2) If $J(G) = J(E)$ (the materials with $\nu_0 = 0.2$), $\nu = \nu_0$, the effective Poisson's ratio of the porous material is independent on
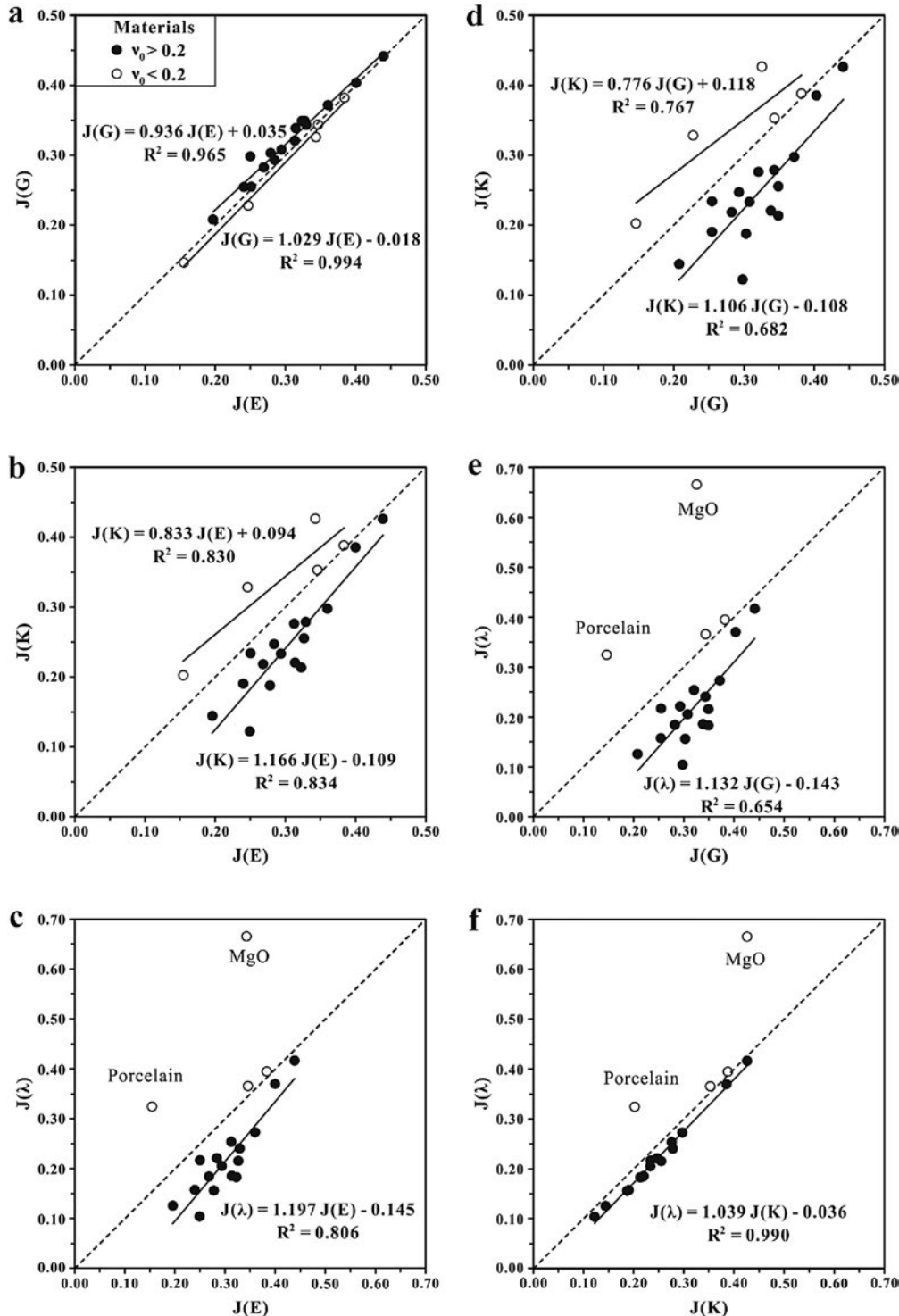

Fig. 13. Correlations among the $J(E)$, $J(G)$, $J(K)$ and $J(\lambda)$ values for the porous materials studied. Solid dots: $\nu_0 > 0.2$; Open dots: $\nu_0 < 0.2$.

porosity, and thus remains invariable with change in pressure (Wang and Ji, 2009). The Poisson's ratio displays a fixed point at $\nu = \nu_0 = 0.2$ (Fig. 13a).

(3) If $J(G) < J(E)$ (the materials with $\nu_0 < 0.2$, Fig. 12a), $(1-p)^{1/J(E)-1/J(G)} > 1$, then $\nu > \nu_0$. In this case, the effective Poisson's ratio of the porous material increases with increasing porosity (Figs. 4, 6, 8 and 10) and should thus decrease with increasing hydrostatic pressure because the latter decreases the porosity.

Using the Mori and Tanaka (1973) mean-field approach, Dunn and Ledbetter (1995) analyzed theoretically the effective Poisson's ratio of macroscopically isotropic solids containing randomly distributed and randomly oriented spherical, needle-shape or disk-shape pores. They reported that the fixed point of Poisson's ratio changes with the aspect ratio of pores (α: width/length). For the materials containing spherical ($\alpha = 1$) and needle-shape ($\alpha \gg 1$), the fixed point of Poisson's ratio is at $\nu = \nu_0 = 0.2$. For the materials containing disk-shape pores ($\alpha < 1$), however, the fixed point of Poisson's ratio decreases nonlinearly with decreasing pore aspect ratio (Fig. 14). For the extremely thin disk-shape pores ($\alpha \rightarrow 0$), the fixed point is at $\nu_0 \rightarrow 0$. For all the materials described in Section 3, the fixed point of Poisson's ratio is clearly at $\nu = \nu_0 = 0.2$ (Fig. 11a), indicating that the pores in the isostatically hot-pressed, sintered polycrystalline materials (e.g. metals, ceramics, and glasses) and natural quartz sandstones are dominated by corner-shaped holes rather than thin disk-shape pores. The materials containing the corner-shaped holes seem to have the same fixed point of Poisson's ratio at $\nu = \nu_0 = 0.2$ as those containing spherical or tubular pores.

As discussed by Wang and Ji (2009), the presence of thin-disk-shaped pores in a solid material with $0 < \nu_0 < 0.5$ always reduces its effective Poisson's ratio, and displays an effect much more pronounced for the materials with a larger ν_0. Furthermore, the thin-disk-shaped pores with a smaller α value play a much more important role in the reduction of the effective Poisson's ratio than those with a larger α value (Wang and Ji, 2009). Natural rocks in the upper crust, which may be different from the intact samples of man-made materials used in the laboratory, contain often thin-disk-shaped microcracks including intragranular cracks (e.g. cleavage cracks in amphibole, feldspar, mica and pyroxene; intragranular cracks in garnet and quartz) and intergranular cracks (e.g.
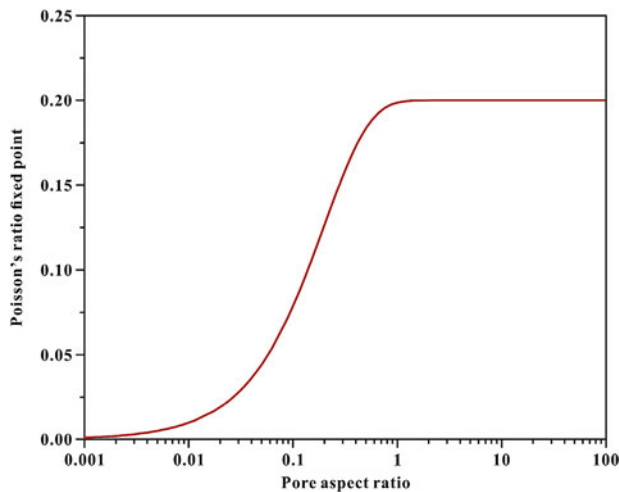
grain boundary cracks, foliation-parallel cracks, lineation-perpendicular or oblique cracks). The smaller the α value, the easier to close the thin-disk-shaped microcracks by hydrostatic pressure. With increasing depth or pressure, the thin-disk-shaped microcracks with smaller α values are progressively closed, and the Poisson's ratio fixed point increases and will finally reach to the point at $\nu = \nu_0 = 0.2$. Below and above the fixed point, the effective Poisson's ratio increases and decreases with increasing porosity, respectively.

5. Conclusions

The studies on the porosity-dependence of elastic and seismic properties of natural rocks are extremely difficult because the geometrical shape, size distribution and connectivity of pores in three-dimensional, opaque rocks are generally unknown. For this reason, experimental results from isotropic man-made materials (e.g. metals, oxides, ceramics and glasses) with calibrated porosities are particularly important for better understanding of seismic data from the natural rocks. In the present study, we used the GMR, which is a simple but rigorous mathematical expression, to provide a unified description for the best fitting relationship between the overall elastic properties (e.g. elastic constants, and seismic velocities) and the porosity in solid materials such as silver, iron, porcelain, fused glass beads, silica glasses, alumina, periclase, spinel and quartz sandstone. The characteristic J value of the GMR, which is regarded as the microstructural coefficient, is controlled mainly by the shape, size distribution, continuity and connectivity of the pores in the solid medium. The most interesting finding is that the J values for Young's (E), shear (G) and bulk (K) moduli and Lame parameter (λ) for a given porous material are systematically different and display some consistent correlations with the Poisson's ratio of the nonporous material (ν_0). For the intact samples of metals, ceramics, glasses and rocks containing dominantly corner-shaped holes, the Poisson's ratio fixed point is at $\nu = \nu_0 = 0.2$. In other words, $J(G) > J(E) > J(K) > J(\lambda)$ for the the materials with $\nu_0 > 0.2$ while $J(G) < J(E) < J(K) < J(\lambda)$ for the materials with $\nu_0 < 0.2$. For the materials $\nu_0 = 0.2$, $J(G) = J(E) = J(K) = J(\lambda)$. $J(V_s) > J(V_p)$ for the porous materials with $\nu_0 > 0.2$ whereas $J(V_s) < J(V_p)$ for those porous materials with $\nu_0 < 0.2$. For those materials with $\nu_0 \approx 0.2$, $J(V_s) \approx J(V_p)$. The effective Poisson's ratio increases, decreases and remains invariable with increasing porosity for the materials with $\nu_0 < 0.2$, $\nu_0 > 0.2$ and $\nu_0 = 0.2$, respectively. $J(K)$ displays an excellent correlation with $J(V_p)$ for the materials with $\nu_0 > 0.2$. The dependences of $J(E)$ on $J(V_p)$ and (V_s) are nonlinear and linear, respectively. The $J(\lambda)$ demonstrates nicely a linear relationship with $J(V_p)$ for the materials with $\nu_0 > 0.2$. However, natural rocks in the upper crust, which may be different from the intact samples of man-made materials used in the laboratory, contain generally thin-disk-shaped microcracks such as cleavage cracks in rock-forming minerals, grain boundary cracks, foliation-parallel cracks, lineation-perpendicular or oblique cracks (e.g. Ji et al., 1997; Sun et al., 2012). For these materials containing disk-shape pores, the fixed point of Poisson's ratio decreases nonlinearly with decreasing pore aspect ratio (α: width/length). For the extremely thin disk-shape pores ($\alpha \rightarrow 0$), the fixed point is at $\nu_0 \rightarrow 0$. With increasing depth or pressure, the thin-disk-shaped microcracks with smaller α values are progressively closed, and the Poisson's ratio fixed point increases and will finally reach to the point at $\nu = \nu_0 = 0.2$. Below and above the fixed point, the effective Poisson's ratio increases and decreases with increasing porosity, respectively. The present work provides a foundation upon which to base further studies.

Fig. 14. The fixed point of Poisson's ratio of a porous material as a function of the pore aspect ratio (Modified after Dunn and Ledbetter, 1995).

Conflict of interest

Acknowledgments

References

Adachi T, Sakka S. Dependence of the elastic moduli of porous silica gel prepared by the sol—gel method on heat-treatment. Journal of Materials Science 1990;25(11):4732—7.

Asmani M, Kermel C, Leriche A, Ourak M. Influence of porosity on Young's modulus and Poisson's ratio in alumina ceramics. Journal of the European Ceramic Society 2001;21(8):1081—6.

Barzegari MR, Rodrigue D. The effect of density profile on the flexural properties of structural foams. Polymer Engineering and Science 2007;47(9):1459—68.

Berge PA, Bonner BP, Berryman JG. Ultrasonic velocity-porosity relationships for sandstone analogs made from fused glass beads. Geophysics 1995;60(1):108—19.

Boisson J, Platon F, Boch P. Measurements of elastic constants and an elastic capacity of some ceramics with various porosities. Ceramurgia 1976;6:74—80.

Chevrot S, van der Hilst RD. The Poisson's ratio of the Australian crust: geological and geophysical implications. Earth and Planetary Science Letters 2000;183(1—2):121—32.

Christensen NI. Poisson's ratio and crustal seismology. Journal of Geophysical Research: Solid Earth 1996;101(B2):3139—56.

Clarke TJ, Silver PG. Estimation of crustal Poisson's ratio from broad band teleseismic data. Geophysical Research Letters 1993;20(3):241—4.

Culliton D, Betts A, Carvalho S, Kennedy D. Improving tribological properties of cast Al—Si alloys through application of wear-resistant thermal spray coatings. Journal of Thermal Spray Technology 2013;22(4):491—501.

DiRienzo AL, Yakacki CM, Frensemeier M, Schneider AS, Safranski DL, Hoyt AJ, Frick CP. Porous poly (para-phenylene) scaffolds for load-bearing orthopedic applications. Journal of the Mechanical Behavior of Biomedical Materials 2014;30:347—57.

Dole SL, Hunter O, Wooge CJ. Elastic properties of monoclinic hafnium oxide at room temperature. Journal of the American Ceramic Society 1977;60(11—12):488—90.

Dufour J, Squires J, Goodway WN, Edmunds A, Shook I. Integrated geological and geophysical interpretation case study, and Lamé rock parameter extractions using AVO analysis on the Blackfoot 3C-3D seismic data, southern Alberta, Canada. Geophysics 2002;67(1):27—37.

Dunn ML, Ledbetter H. Poisson's ratio of porous and microcracked solids: theory and application to oxide superconductors. Journal of Materials Research 1995;10(11):2715—22.

Estabrook CH, Kind R. The nature of the 660-kilometer upper-mantle seismic discontinuity from precursors to the PP phase. Science 1996;274(5290):1179—82.

Gercek H. Poisson's ratio values for rocks. International Journal of Rock Mechanics and Mining Sciences 2007;44(1):1—13.

Goodway B. AVO and Lamé constants for rock parameterization and fluid detection. CSEG Recorder 2001;26:39—60.

Goodway B, Chen T, Downton J. Improved AVO fluid detection and lithology discrimination using Lame petrophysical parameters, λρ, μρ, and λ/μ fluid stack, from P and S inversions. In: Canadian Society of Exploration Geophysicists (SEG) Technical Program Expanded Abstracts; 1997. p. 183—6.

Gray D. A better way to extract fundamental rock properties with much less noise. World Oil 2003;224:49—53.

Gray D, Andersen E. Application of AVO and inversion to formation properties. World Oil 2000;221:85—92.

Haglund JA, Hunter O. Elastic properties of polycrystalline monoclinic Gd$_2$O$_3$. Journal of the American Ceramic Society 1973;56(6):327—30.

Han D. Effects of porosity and clay content on acoustic properties of sandstones and unconsolidated sediments. PhD Thesis. Stanford, USA: Stanford University; 1986.

Hunter O, Graddy GE. Porosity dependence of elastic properties of poly-crystalline cubic Lu$_2$O$_3$. Journal of the American Ceramic Society 1976;59(1—2):82.

Hunter O, Korklan HJ, Suchomel RR. Elastic properties of polycrystalline monoclinic Sm$_2$O$_3$. Journal of the American Ceramic Society 1974;57(6):267—8.

Jaeger JC. Elasticity, fracture and flow: with engineering and geological applications. Springer; 1969.

Jeong H, Hsu DK. Quantitative estimation of material properties of porous ceramics by means of composite micromechanics and ultrasonic velocity. NDT & E International 1996;29(2):95—101.

Ji S. A generalized mixture rule for estimating the viscosity of solid-liquid suspensions and mechanical properties of polyphase rocks and composite materials. Journal of Geophysical Research: Solid Earth 2004;109(B10). http://dx.doi.org/10.1029/2004JB003124.

Ji SC, Wang Q, Xia B. Handbook of seismic properties of minerals, rocks and ores. Montreal, Canada: Polytechnic International Press; 2002.

Ji S, Gu Q, Xia B. Porosity dependence of mechanical properties of solid materials. Journal of Materials Science 2006;41(6):1757—68.

Ji S, Li A, Wang Q, Long C, Wang H, Marcotte D, Salisbury M. Seismic velocities, anisotropy and shear-wave splitting of antigorite serpentinites and tectonic implications for subduction zones. Journal of Geophysical Research: Solid Earth 2013a;118(3):1015—37.

Ji S, Shao T, Michibayashi K, Long C, Wang Q, Kondo Y, Zhao W, Wang H, Salisbury M. A new calibration of seismic velocities, anisotropy, fabrics, and elastic moduli of amphibole-rich rocks. Journal of Geophysical Research: Solid Earth 2013b;118(9):4699—728.

Ji S, Zhao P, Saruwatari K. Fracturing of garnet crystals in anisotropic metamorphic rocks during uplift. Journal Structural Geology 1997;19(5):603—20.

Ji S, Sun S, Wang Q, Marcotte D. Lamé parameters of common rocks in the Earth's crust and upper mantle. Journal of Geophysical Research: Solid Earth 2010;115(B6). http://dx.doi.org/10.1029/2009JB007134.

Ji S, Wang Q, Salisbury MH. Composition and tectonic evolution of the Chinese continental crust constrained by Poisson's ratio. Tectonophysics 2009;463(1—4):15—30.

Ji S, Wang Q, Xia B. Mechanical properties of multiphase materials and rocks: a simple phenomenological approach using generalized means. Journal of Structural Geology 2004;26(8):1377—90.

Lakes R. Foam structures with a negative Poisson's ratio. Science 1987;235(4792):1038—40.

Li Y, Downton J, Goodway B. Recent applications of AVO to carbonate reservoirs in the Western Canadian sedimentary basin. The Leading Edge 2003;22(7):670—4.

Luo J, Stevens R. Porosity-dependence of elastic moduli and hardness of 3Y-TZP ceramics. Ceramics International 1999;25(3):281—6.

Martin LP, Dadon D, Rosen M. Evaluation of ultrasonically determined elasticity-porosity relations in zinc oxide. Journal of the American Ceramic Society 1996;79(5):1281—9.

Matikas TE, Karpur P, Shamasundar S. Measurement of the dynamic elastic moduli of porous titanium aluminide compacts. Journal of Materials Science 1997;32(4):1099—103.

McLean AF, Fisher EA. Brittle materials design, high temperature gas turbine. DTIC Document. 1981.

Mori T, Tanaka K. Average stress in matrix and average elastic energy of materials with misfitting inclusions. Acta Metallurgica 1973;21(5):571—4.

Nair SK, Gao SS, Liu KH, Silver PG. Southern African crustal evolution and composition: constraints from receiver function studies. Journal of Geophysical Research: Solid Earth 2006;111(B2). http://dx.doi.org/10.1029/2005JB003802.

Owens TJ, Zandt G. Implications of crustal property variations for models of Tibetan plateau evolution. Nature 1997;387:37—43.

Pal R. Porosity-dependence of effective mechanical properties of pore-solid composite materials. Journal of Composite Materials 2005;39(13):1147—58.

Panakkal JP, Willems H, Arnold W. Nondestructive evaluation of elastic parameters of sintered iron powder compacts. Journal of Materials Science 1990;25(2):1397—402.

Panakkal JP. Use of longitudinal ultrasonic velocity as a predictor of elastic moduli and density of sintered uranium dioxide. IEEE Transactions on Ultrasonics, Ferroelectrics and Frequency Control 1991;38(3):161—5.

Porter DF, Reed JS, Lewis III D. Elastic moduli of refractory spinels. Journal of the American Ceramic Society 1977;60(7—8):345—9.

Shao T, Ji S, Kondo Y, Michibayashi K, Wang Q, Xu Z, Sun S, Marcotte D, Salisbury M. Antigorite-induced seismic anisotropy and implications for deformation in subduction zones and the Tibetan Plateau. Journal of Geophysical Research: Solid Earth 2014;119(3):2068—99.

Smith CF, Crandall WB. Calculated high-temperature elastic constants for zero porosity monoclinic zirconia. Journal of the American Ceramic Society 1964;47(12):624—7.

Soga N, Schreiber E. Porosity dependence of sound velocity and Poisson's ratio for polycrystalline MgO determined by resonant sphere method. Journal of the American Ceramic Society 1968;51(8):465—7.

Sun S, Ji S, Wang Q, Salisbury M, Kern H. P-wave velocity differences between surface-derived and core samples from the Sulu ultrahigh-pressure terrane: implications for in situ velocities at great depths. Geology 2012;40(7):651—4.

Takeda YT, Griera A. Rheological and kinematical responses to flow of two-phase rocks. Tectonophysics 2006;427(1—4):95—113.

Tarkov AP, Vavakin VV. Poisson's ratio behaviour in various crystalline rocks: application to the study of the Earth's interior. Physics of the Earth and Planetary Interiors 1982;29(1):24–9.

Wang Q, Ji S. Poisson's ratio of crystalline rocks as a function of hydrostatic confining pressure. Journal of Geophysical Research: Solid Earth 2009;114(B9). http://dx.doi.org/10.1029/2008JB006167.

Yeheskel O, Shokhat M, Ratzker M, Dariel MP. Elastic constants of porous silver compacts after acid assisted consolidation at room temperature. Journal of Materials Science 2001;36(5):1219–25.

Yu Y, Wu XP. Study of the generalized mixture rule for determining effective conductivity of two-phase stochastic models. Applied Geophysics 2010;7(3):210–6.

Zandt G, Ammon CJ. Continental crust composition constrained by measurements of crustal Poisson's ratio. Nature 1995;374:152–4.

Chengbo Yu obtained a Bachelor of Engineering degree from the School of Architecture and Civil Engineering, Beijing University of Technology (China) in 2008, and a Master of Engineering degree from Ecole Polytechnique de Montreal (Canada) in 2014. During his study in Montreal, he was involved in research on seismic velocities, elastic moduli and Poisson's ratios of solid materials and rocks as a function of porosity and pore geometry. His research was under the direction of Prof. Shaocheng Ji.